Clustering instability in a freely falling granular jet

Matthias E. Möbius
The James Franck Institute and Department of Physics, The University of Chicago, Chicago, Illinois 60637, USA
(Received 7 March 2006; revised manuscript received 9 August 2006; published 14 November 2006)

This paper investigates a clustering instability of a freely falling granular jet composed of 100 μm glass spheres. The granular flow out of a circular nozzle starts out spatially uniform and then, further downstream, breaks up into well-defined clusters. An optical method is used that measures inhomogeneities in the flow in order to quantify the growth of the clusters. The role of air is investigated in this phenomenon by changing the ambient air pressure down to 1/5000th atm. Clustering is observed down to the lowest pressure and the presence of air leads to larger clusters but does not initiate the cluster formation. The analysis shows that the cluster size is set by fluctuations on the order of the size of the particles at the nozzle.

DOI: 10.1103/PhysRevE.74.051304 PACS number(s): 45.70.−n, 83.60.Wc, 47.50.Gj

I. INTRODUCTION

Granular media often appear to behave like ordinary fluids. One can pour sand into a bucket or let it flow down an inclined plane. This paper investigates how a freely falling granular jet emanating from an aperture becomes inhomogeneous and starts to form clusters (Fig. 1) similar to an ordinary fluid column breaking up due to the Rayleigh-Plateau instability [1]. Despite this apparent similarity in behavior there are considerable differences between fluid and granular flows. The fluid jet instability is driven by the surface tension of the liquid. Dry, noncohesive granular media, however, do not possess surface tension, so it is not obvious how this granular jet becomes unstable and forms clusters.

Due to the lack of surface tension, the clustering instability must be driven by something else. In general, inhomogeneities in granular flows are quite common due to friction between particles and geometrical constraints imposed by boundaries. This can lead to arching and jamming. In the case studied here, however, the clusters form *in the absence* of boundaries. This distinguishes it from other clustering phenomena in granular flows such as density waves in funnels and vertical pipes [2–7].

The clustering of freely falling granular jets appears to be generic. Recent experiments revealed that after the impact of a large sphere on a loosely packed bed of small particles a surprisingly tall granular jet emerges [8–10]. Subsequently, the jet breaks up into clusters whose size is comparable to the jet diameter. This is another example of clustering in the absence of nearby boundaries.

This study investigates, as a function of air pressure, cluster formation from the flow out of a funnel. Air is important when dealing with small grains. Viscous drag can easily exceed the particle's weight for the 100 μm glass spheres used in this experiment. Moreover, investigating the role of air enables a comparison with recent experiments on cluster formation in an underwater granular jet [11,12]. In the experiment presented here we can tune the influence of the surrounding "liquid"—namely the air. In particular the properties of the clusters are studied, such as their size and growth as they freely fall, as a function of pressure.

The typical cluster size decreases with decreasing pressure and then saturates below 0.1 kPa. Thus, air influences the clustering but is not necessary for initiating the process. At all pressures the clusters grow as they fall. The growth is well fit with a gravitational stretching function which indicates that perturbations of the order of a grain size at the nozzle serve as nucleation points for the clusters. At higher pressures the jet disintegrates into a particle cloud below some depth. The depth at which disintegration occurs increases with decreasing pressure. At the lowest available pressure, $p \approx 1/5000$th atm, the jet does not disintegrate within the experimentally accessible range of depth (2.1 m).

The following section gives an overview of inhomogeneities that can arise in granular flows. Section III describes the experimental method. The next section contains the experimental results and is followed by a discussion and conclusion in Secs. V and VI.

II. BACKGROUND

Intermittency and clogging are intrinsic features of granular flows. This is due to friction between grains and geometric constraints that prevent grains from flowing past each other when the flow is confined by boundaries (jamming). For finer particles air can also induce intermittency. This is observed in various systems, such as flow down a vertical pipe or in hourglasses [3–7,13]. In the experiment presented here the system undergoes a change from a dense granular funnel flow to a freely falling flow. Both regimes are susceptible to intermittency and clustering. In the following, different mechanisms that create inhomogeneities in granular flows and gases are reviewed.

A. Density waves

Density fluctuations can propagate through a flow, such as in vertical pipes [3,4] or funnel flow. Granular funnel flow and the related hopper flow have been extensively studied in the literature. The flow out of a nozzle can become inhomogeneous in a two-dimensional as well as a three-dimensional funnel system [2,14]. As the grains move downward under the influence of gravity, arches form near the nozzle that can temporarily hold up the flow before they collapse. The presence of these density waves is enhanced when the grains are rough and is suppressed when the grains are smooth spheres [2].

B. Interstitial fluid effects

Apart from grain-grain and grain-boundary interactions, interstitial gas can profoundly affect the flow. This is espe-

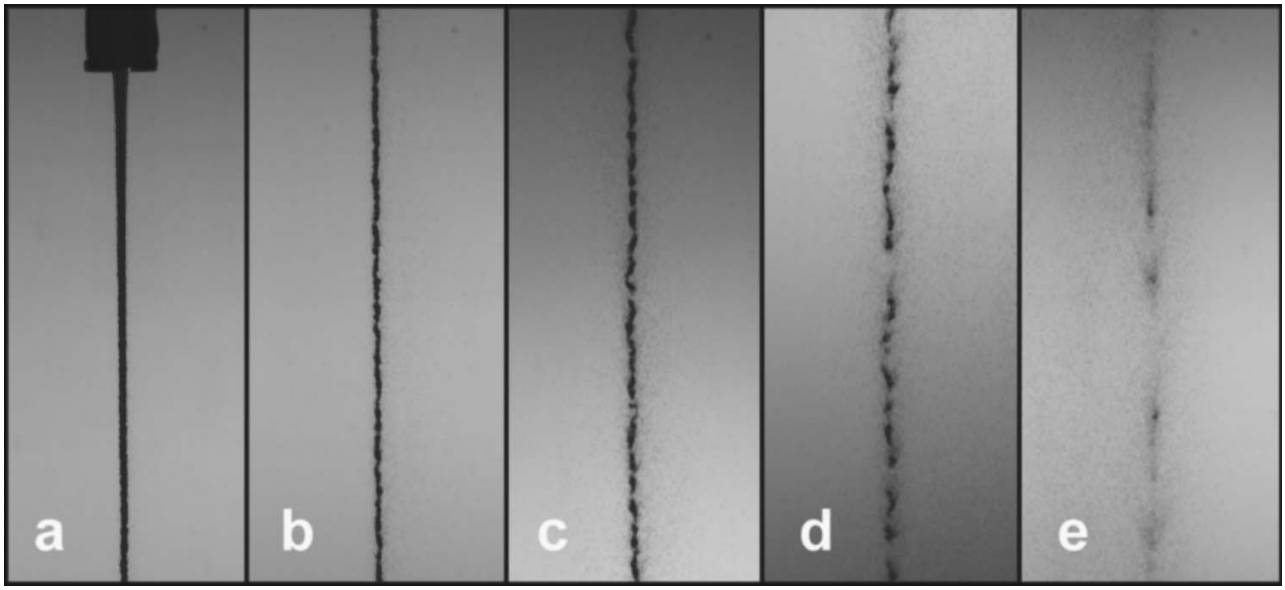

FIG. 1. 100 micron glass spheres draining from the 4 mm wide circular nozzle at atmospheric pressure. This porous funnel is the same as used in the experiment. Pictures are taken at different depths z below the nozzle. (a) At the nozzle, (b) $z=25$ cm, (c) $z=55$ cm, (d) $z=75$ cm, (e) $z=130$ cm.

cially important for systems where the particle size is well below 1 mm [15]. In this regime viscous drag and pressure gradients inside the bed can strongly influence the dynamics. In typical experimental settings ($v \lesssim 1$ m/s, $p=1$ atm) this effect does not matter much for grain sizes $\gtrsim 1$ mm, but becomes important for smaller media such as the 100 μm glass spheres used in this experiment. As a result, the granular flow out of an aperture can become oscillatory [6,7,13]. This so-called "ticking" is due to pressure gradients inside the bed that create a back-flow of air into the nozzle.

In cases where the interstitial fluid is a liquid, interesting flow instabilities have been observed [11,12]. Nicolas [12] also studied a granular jet emanating from a nozzle, but in the presence of a liquid. Depending on the grain and liquid parameters, the jet can either remain homogeneous or become unstable and form blobs similar to the clusters shown in Fig. 1. The origin of this instability still remains unclear. Nicolas showed that treating the suspension jet as a fluid with some effective viscosity cannot explain this instability.

C. Inelastic clustering

A granular gas is dissipative due to the inelastic nature of the collisions between the grains. Therefore, without external energy supply the gas cools down with time and eventually freezes [16–18]. However, it does not cool homogeneously, but forms clusters. When a fluctuation increases the density locally, the collision rate goes up in this region. Due to the increased dissipation, the granular temperature decreases which in turn lowers the pressure. The resulting pressure gradient will enhance migration of particles into that region, thereby increasing the density even further. Eventually, these regions grow into clusters.

D. Cohesion

Humidity in the air and surface charges can induce cohesive forces between particles [15]. Condensates from ambient humidity create liquid bridges causing particles to stick together. As with interstitial fluid effects, the influence of cohesion depends strongly on the size and the density of the particles. Smaller and lighter media are more susceptible to cohesive forces. Cohesion does not cause intermittency per se, but can dramatically change the rheological properties of granular media. In extreme cases it leads to clumping and caking. These effects can be controlled but not completely eliminated. Even dry grains, as used in this experiment, may still experience some small residual cohesive forces that could potentially induce clustering in the freely falling jet.

III. EXPERIMENTAL METHOD

In this paper all experiments have been performed with monodisperse ($d=100$ μm) spherical glass beads (Mo-Sci Corp., $\rho=2500$ g/l) (Fig. 1). In order to investigate the clustering in the emerging jet quantitatively, an optical system was set up to measure inhomogeneities in the jet—similar to ones used in previous studies for measuring intermittent granular flows in hourglasses and vertical pipes [3,5,7]. The basic idea is to measure the light intensity of a laser shining through the falling grains. The fluctuations in the intensity correspond to the inhomogeneities in the flow. This method does not measure density variations, but rather the emergence of undulations on the jet surface and gaps.

The schematics of the setup are shown in Fig. 2. The funnel is mounted inside and near the top of a 14 cm wide acrylic tube whose diameter is large enough so that the particles are always far from the wall. A 9 cm wide cylindrical reservoir feeds the grains into a tube made of metal mesh. At the bottom of this tube a disc with a 4 mm circular aperture is attached from which the particles emerge and then freely fall down the tube. There is a remote controlled shutter beneath the nozzle to initiate and stop the flow. The pressure

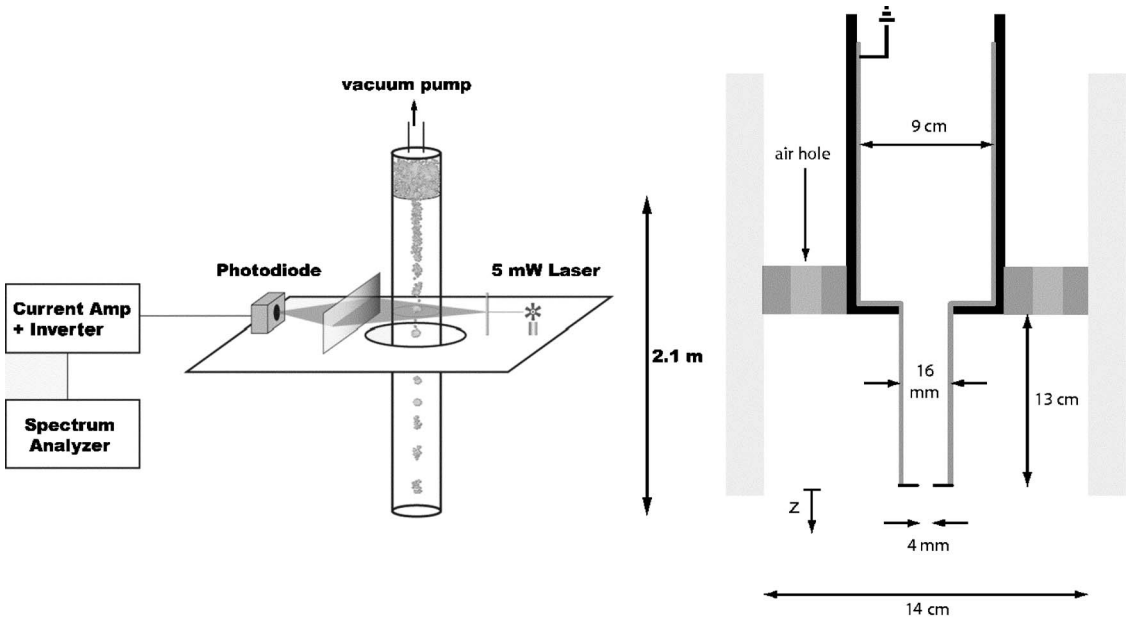

FIG. 2. Left-hand side: The setup. The granular jet emerges from the reservoir at the top of the 14 cm wide acrylic tube. The tube is connected to a vacuum pump and the pressure is measured with a pressure gauge mounted on the lid. The optical platform can be adjusted to any height between the nozzle and 2.1 m below. The light from a 5 mW (λ=650 nm) laser diode is focused by a lens, then passed through a glass rod to spread it out and finally refocussed with a cylindrical lens onto a photodiode. An identical laser sheet (not shown) is mounted 5.1 mm below the first sheet. The signals of the two photodiodes are passed to two current amps that also invert the signals. The two signals are cross correlated with a spectrum analyzer and one of them is sent to an A/D converter card. Right-hand side: Schematics of the reservoir and the funnel. The reservoir consists of a 9 cm wide acrylic tube which feeds a 16 mm wide porous tube. At the bottom of the porous tube a metal disc is attached with a 4 mm circular aperture. The inside is covered with metal mesh and is grounded. The reservoir sits on a ring that has several holes in it to allow for pressure equalization between the reservoir and the lower part of the tube. The depth z is measured from the nozzle.

inside the acrylic tube can be pumped down to 0.02 kPa. For air, this corresponds to a mean free path of 0.3 mm ($\approx$3 d) [19]. The pressure is monitored with a pressure gauge mounted on the lid (Granville-Phillips, Convectron gauge 375). An oil filter (K.J. Lesker micromaze foreline trap) and a shut-off valve was installed between the system and the vacuum pump to avoid contamination of the system with oil vapor that might emanate from the vacuum pump.

A prerequisite for this experiment is to ensure a steady nonchanging flow out of the nozzle. It is known that air pressure gradients across the bed can cause oscillatory flow ("ticking") out of the nozzle [13]. Even equalizing the pressure in the reservoir with the pressure at the nozzle is not sufficient for steady flow conditions. To eliminate ticking, the tube coming from the reservoir is made out of metal mesh (0.0014 in. wire mesh 325×325) that is permeable to air, but not to the particles, thereby allowing pressure equalization through the boundaries (Fig. 2). This ensures a stable flow rate at all pressures.

The whole optical system is mounted on a platform that is moveable in the vertical direction and can be lowered to 2.1 m below the nozzle. Since the width of the freely falling particle flow exceeds the diameter of the laser beam (5 mW laser diodes from z-bolt.com), the light is spread out to a sheet to capture the entire horizontal spread of the flow. This is achieved by shining the light through a 8 mm diameter glass rod. The beam is also focused in the horizontal plane by a lens to ensure that the beam waist is smaller than the emerging structures. The vertical width is 0.3 mm ($\approx3d$). After the laser sheet passes through the particle flow, it is refocused by a cylindrical lens onto a photodiode (Silonex SLD-68HL1D) that measures the intensity. A current amp is used to convert the diode current, which is linearly proportional to the incident light intensity, into a voltage signal. The signal is inverted since the quantity of interest is the amount of light that is screened by the jet. In the following this signal is referred to as the blockage B. The frequency response is flat up to at least 100 kHz. The signal is recorded with an A/D converter card at a sampling rate of 48 kHz. The baseline of the signal changes with vertical position due to imperfections of the acrylic tube. The signal is scaled with the baseline at each position before each experimental run.

In order to convert time scales into length scales, the local average velocity of the flow is measured by cross correlating the intensity signal of two closely spaced laser sheets (vertical distance =5.1 mm). In order to avoid cross-talk between the two photodiodes through scattered light a shutter is mounted near the cylindrical lens. A 2-channel spectrum analyzer (SRS SR780) obtains the cross correlation between the two signals in real time.

When calculating autocorrelations, the mean of the signal is subtracted and the autocorrelation is normalized to 1 at zero time delay Δt. In that way, the autocorrelation approaches zero at large Δt. Near the nozzle, the signal to noise is low and a noise floor appears in the autocorrelation. The electric noise floor is measured directly by obtaining the au-

tocorrelation of the laser signal without the granular jet. It is then subtracted from the autocorrelation.

Cohesion between particles is caused by liquid bridges and/or electrostatic interaction due to charge buildup [15]. The latter is especially significant in dry atmospheres. Avoiding charge build-up in the grains is crucial in this experiment. To ensure stable conditions the laboratory is controlled at 50% relative humidity, which provides enough ions to neutralize surface charges, but does not result in clumping. Moreover, the walls of the reservoir are grounded to avoid build up of charge through friction. After each run, the beads are exposed to ionized air to neutralize any charges that might have built up during the run. For runs at low pressures the humidity vanishes in the tube. However, the previous exposure to the ionized air and the humidity controlled environment is sufficient to ensure stable conditions. At low pressures, no drift in cluster size has been observed over the course of the experiment.

IV. RESULTS

In order to compare the clustering at different pressures we need to know the flow rate out of the nozzle and the velocity of the jet as a function of pressure. As mentioned above, a porous tube is used to ensure steady flow at higher pressures. Furthermore, care has been taken to prepare the glass spheres in the reservoir in the same way after each run so that the packing fraction remains constant. In all runs the filling height was kept above a minimum height beyond which the flow rate was height independent (Janssen effect). The flow rate is nearly constant at all pressures: At atmospheric pressures the flow rate is 1.82 cm^3/s, which is slightly lower than at $p=0.04$ kPa, where it is 1.87 cm^3/s. This few percent difference is negligible for the subsequent analysis. The constant flow rate allows a direct comparison of the clustering at different pressures. In order to convert the signals recorded in the time domain into the length domain, we need to know the velocity at each height. Figure 3 shows the velocity of the jet versus depth at four pressures. In the absence of any hydrodynamic drag force the velocity v should just follow $v=\sqrt{2gz+v_0^2}$, where z is the distance as measured from the aperture, v_0 the velocity at the nozzle and g is the acceleration of gravity. When $(v^2-v_0^2)/2$ is plotted against the depth z, the resulting curve is linear for simple free fall with a slope equal to the acceleration $a=g$. v_0 is constant within a few percent at all pressures. This is consistent with the constant flow rate found earlier. Down to the lowest available pressure we find a linear relationship between $(v^2-v_0^2)/2$ and z with a slope close to or equal to g. At higher pressures deviations are observed when the jet starts to disintegrate into a cloud of particles [Fig. 1(e)]. When $p=101$ kPa (=1 atm), this happens around 1.2 m below the nozzle [Fig. 3(d)]. At this point the mean velocity stops growing with depth and the previously sharp cross-correlation peak becomes broad. When the pressure is lowered, the disintegration starts further downstream [Fig. 3(c)]. At the lowest pressure [Fig. 3(a)], no disintegration is observed in the experimentally available range of depth.

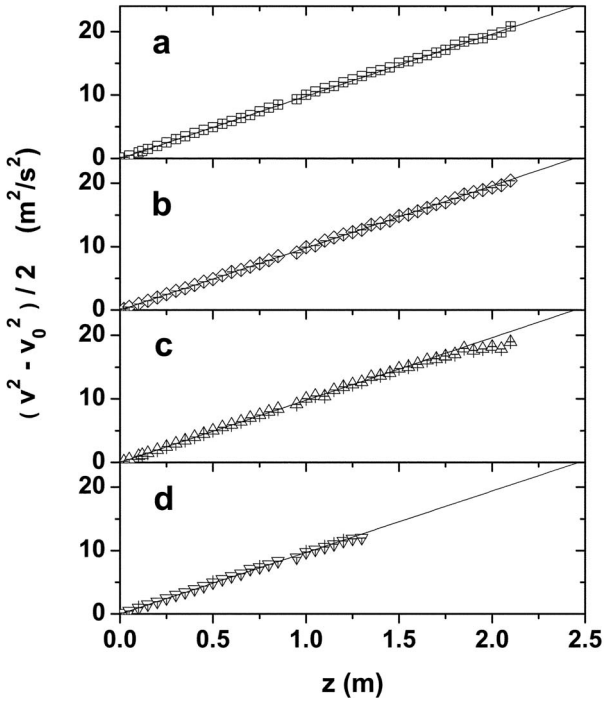

FIG. 3. Velocity of the jet versus depth at different pressures. In all panels, $v_0=0.36$ m/s. The solid lines are linear fits to the data. The slope represents the acceleration a. (a) $p=0.027$ kPa, $a=9.8$ m/s; (b) $p=0.67$ kPa, $a=9.8$ m/s; (c) $p=49$ kPa, $a=9.8$ m/s; (d) $p=101$ kPa, $a=9.7$ m/s.

The low drag on the jet at $p=101$ kPa is surprising given that the viscous drag on a single grain is substantial and would lead to a terminal velocity of 0.76 m/s according to the Stokes formula for viscous drag on a sphere: $F_{\text{Stokes}}=3\pi\mu dv$. A possible explanation is that the air is essentially trapped inside the jet so that it appears solid. Treating the jet as a porous medium, one can estimate the time it takes for air to penetrate the jet. Inside a porous medium, the pressure obeys a diffusion equation [20]. The diffusion constant is $D=(P_0k)/[\mu(1-\phi)]$, where P_0 is the ambient gas pressure, μ is the dynamic viscosity of air, and k is the permeability of the granular medium at a packing fraction ϕ. The permeability is an empirical constant that is well approximated by the Carman-Kozeny relation [20]: $k=d^2(1-\phi)^3/(180\phi^2)$. The value for D is 0.3 m^2/s after substituting numerical values for the constants: $\mu=1.8\times10^{-5}$ Pa s, $P_0=101$ kPa, and $\phi=0.5$. The latter is a typical packing fraction for a random loose pack of spheres. This value decreases as the jet falls and gets stretched. The typical time τ for air to diffuse into the jet is therefore $\tau\approx r_{jet}^2/(2D)=6.7$ μs. This is small compared to other typical time scales of the system, such as the time it takes for a grain to fall from its own diameter, $d/v\approx10^{-4}$ s. This means that the jet is permeable to air. Therefore, a more sophisticated hydrodynamic description is needed to explain the low drag on the jet at atmospheric pressure.

Figure 4 displays typical time traces of the signal at $p=0.027$ kPa and atmospheric pressure, respectively. At low pressure the evolution of the time trace with depth is as fol-

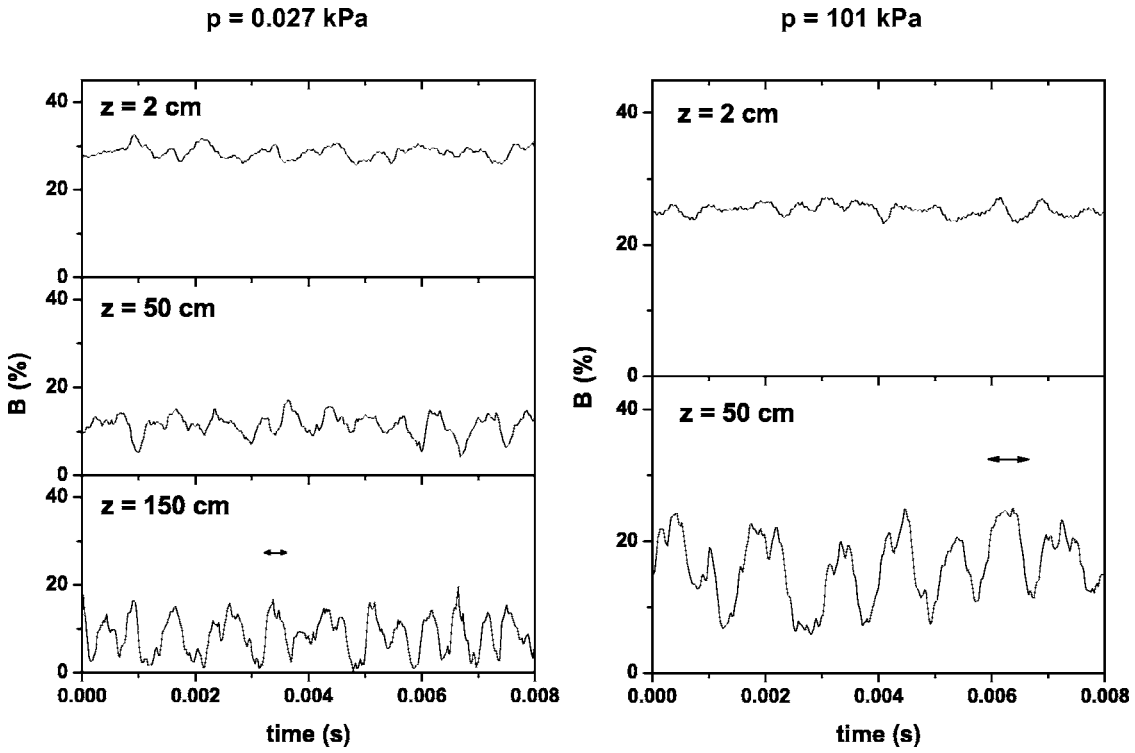

FIG. 4. Blockage at different depths, z, at $p=0.027$ kPa (left-hand panel) and $p=101$ kPa (right-hand panel). The length of the arrow equals the dip position of the corresponding autocorrelation.

lows: Just below the nozzle, $z=2$ cm, clusters have not yet formed and the signal fluctuates only slightly. At $z=50$ cm the fluctuations have visibly increased and finally, at $z=150$ cm, the signal contains clear peaks which show the presence of well-defined clusters. At atmospheric pressure the behavior is similar. Comparing the time traces at $z=50$ cm, it is apparent that the clusters are larger at atmospheric pressure. In atmosphere only depths up to ≈ 120 cm can be probed, since the jet disintegrates beyond that depth.

In order to illustrate the evolution of the clusters, the fluctuations of the blockage signal as a function of depth have been plotted [Fig. 5(a)]. The fluctuations are just the standard

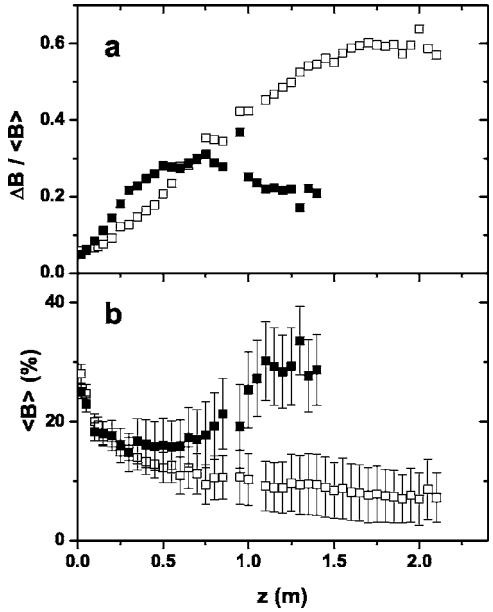

FIG. 5. (a) Blockage fluctuations as a function of depth at two different pressures: (□) $p=0.027$ kPa; (■) $p=101$ kPa. (b) Mean of the blockage as a function of depth at the respective pressures. The error bar delineates the standard deviation ΔB.

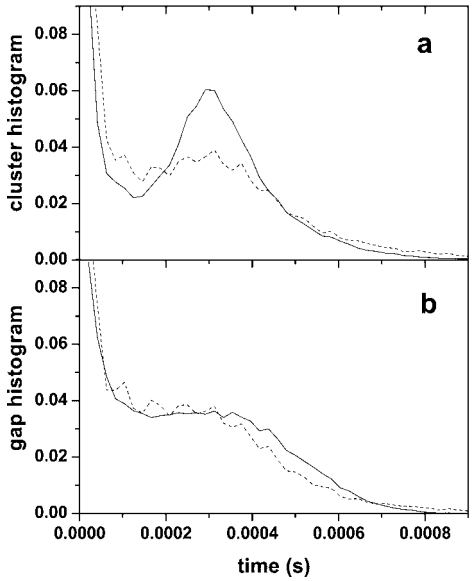

FIG. 6. Histogram of clusters and gaps at $p=0.027$ kPa. In both panels the solid line corresponds to $z=150$ cm and the dashed line to $z=50$ cm. The threshold to discriminate between clusters and gaps is the average of the signal. (a) Cluster histogram; (b) gap histogram.

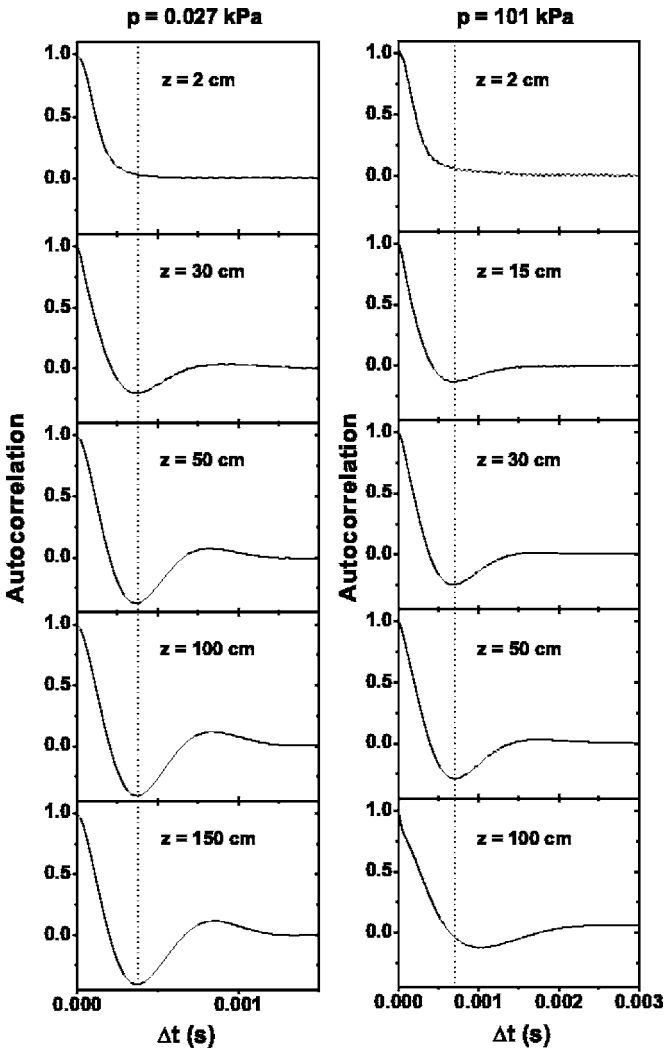

FIG. 7. Autocorrelation at different heights. Left-hand panels show data at $p=0.027$ kPa, the right-hand panels at $p=101$ kPa. The depth at which the signal was recorded is shown in each panel. The vertical dotted lines indicate the dip positions used to calculate λ_0. At $p=0.027$ kPa the dip position does not change with depth.

deviation, ΔB, divided by the mean of the signal $\langle B \rangle$. In vacuum the fluctuations increase monotonically with depth and then saturate. Similarly, at atmospheric pressure the fluctuations increase, but then slowly decrease.

Figure 5(b) shows how $\langle B \rangle$ and ΔB vary with depth. At low pressure, the mean decreases with depth while the standard deviation increases. This reflects the increase of undulations and gaps with increasing depth. At atmospheric pressure, the mean varies nonmonotonically. Beyond 1 m it even exceeds the value at small depth when the jet is still compact. The standard deviation, however, stops increasing far away from the nozzle.

The reason for this marked difference in behavior is that in the presence of air, the jet does not stay collimated far away from the nozzle as it does at low pressures. This leads to an increased blockage as the jet starts to spread. Furthermore, there is more spray, presumably caused by advection of particles by the surrounding air. The optical signal is sensitive to this spray since it scatters the light. This explains why the mean blockage starts to rise again below 60 cm or so. It should also be noted that even if the jet is still homogeneous, the blockage does not reach 100% at both pressures, since the laser sheet is wider than the jet diameter.

One way to analyze the signal is to choose a threshold and convert the blockage signal into a binary sequence as done by Raafat and co-workers [5]. Anything above the threshold is considered a cluster, anything below a gap. The resulting histogram is shown in Fig. 6. This was obtained at $p=0.027$ kPa for two heights and the threshold was taken to be the signal average. The cluster histogram displays a clear peak at $z=150$ cm, while it is less pronounced at $z=50$ cm. The gap histogram remains flat and falls off at large gap sizes in both cases. The high occurrence of very small cluster and gap sizes is due to electronic noise and particle spray. The histograms bear some resemblance to the ones in the vertical pipe flow studied by Raafat *et al.* [5]. In summary, Fig. 6 shows the emergence of a typical cluster size, while the gap size distribution is broad.

This analysis is prone to noise. The peak in the cluster histogram appears only below 50 cm, even though inhomogeneities appear earlier (by visual inspection with a stroboscope). A more sensitive analysis is the autocorrelation as shown in Fig. 7.

Autocorrelations are displayed for two different pressures. At both pressures, a dip and a peak in the autocorrelation develops, though the peak is far less pronounced at $p=101$ kPa. The dip position does not change with depth at $p=0.027$ kPa. At atmospheric pressure, the dip remains constant as a function of depth initially, but then moves to higher Δt below $z=80$ cm. Also, the dip position at $p=101$ kPa is significantly larger than at low pressure. At low depths ($z<80$ cm) it is 7.0×10^{4} s compared to 3.8×10^{-4} s at $p=0.027$ kPa.

A priori it is not clear whether the dip represents the time scale of clusters or gaps. Looking at the time traces in Fig. 4, clusters and gaps have similar sizes. The histogram (Fig. 6) confirms this observation. The cluster and gap size distribution are both broad and fall off around 0.008 s. Therefore, the dip reflects the typical size of the fluctuations in the time domain. The length of the arrows in Fig. 4 represents the dips in the respective autocorrelations of the time traces. They show good agreement with the typical fluctuation size by visual inspection.

Summarizing the above, we identify the dip position with the typical fluctuation size (in the time domain) and find that with increasing depth it stays constant for low pressures and becomes larger for atmospheric pressure. Converting the dip position into a length scale it follows that the clusters and gaps continually grow as they fall.

In order to understand the growth of the clusters it is instructive to consider the case where the jet is just stretched due to gravity ignoring all other interactions. The equations of motion for two grains, one right at the nozzle starting with velocity v_0, the other a distance λ_0 below, are, respectively,

$$z = v_0 t + \frac{1}{2} g t^2, \tag{1}$$

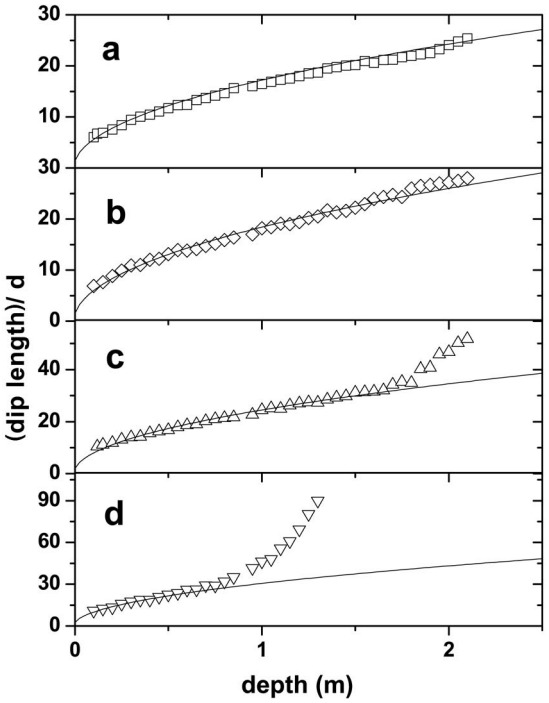

FIG. 8. Dip length vs depth at different pressures. Each dip position has been converted into a length scale by multiplying it with the local velocity. The solid lines are fits from Eq. (3). The error bars are the size of the symbols. (a) $p=0.027$ kPa; (b) $p=0.67$ kPa; (c) $p=49$ kPa; (d) $p=101$ kPa.

$$z' = \lambda_0 + v_1 t + \frac{1}{2} g t^2, \tag{2}$$

where $v_1=\sqrt{2g\lambda_0+v_0^2}$ is the velocity the grain attains by falling a distance λ_0. Due to gravitational acceleration the initial grain separation λ_0 will grow in time as $\lambda(t)=z'-z$.

Parametrizing t with z we obtain

$$\lambda(z) = \lambda_0 + \frac{v_0^2}{g}\left(\sqrt{\frac{2g\lambda_0}{v_0^2}+1}-1\right)\left(\sqrt{\frac{2gz}{v_0^2}+1}-1\right). \tag{3}$$

When $\lambda_0 \ll \frac{v_0^2}{2g}$ this reduces to

$$\lambda(z) = \lambda_0\sqrt{\frac{2gz}{v_0^2}+1}. \tag{4}$$

Far away from the nozzle, when $z \gg \frac{v_0^2}{2g}$, this can be further simplified to

$$\lambda(z) = \lambda_0\frac{\sqrt{2gz}}{v_0}. \tag{5}$$

Since $\sqrt{2gz}$ is just the velocity $v(z)$ at depth z for $z \gg \frac{v_0^2}{2g}$, Eq. (5) can be written as

$$\frac{\lambda_0}{v_0} = \frac{\lambda(z)}{v(z)} \equiv T, \tag{6}$$

where T is the time it takes to fall a distance $\lambda(z)$ at depth z. This time is constant for $z \gg \frac{v_0^2}{2g}$. We can now compare T with the dip position of the autocorrelation which is a measure of how long it takes for a cluster to fall. At $p=0.027$, the dip position is constant at all depths to within a few percent: 3.8×10^{-4} s; the clusters just get stretched by falling in gravity. The velocity at the nozzle is $v_0=0.36$ m/s. Therefore, $\lambda_0=1.4\times10^{-4}$ m$=1.4d$ (this also justifies the approximation $\lambda_0 \ll \frac{v_0^2}{2g}$ to simplify Eq. (3)). At atmospheric pressure the dip position is larger and grows below $z=80$ cm. Using the value of the dip position for smaller depths, we find $\lambda_0=2.5\times10^{-4}$ m$=2.5d$.

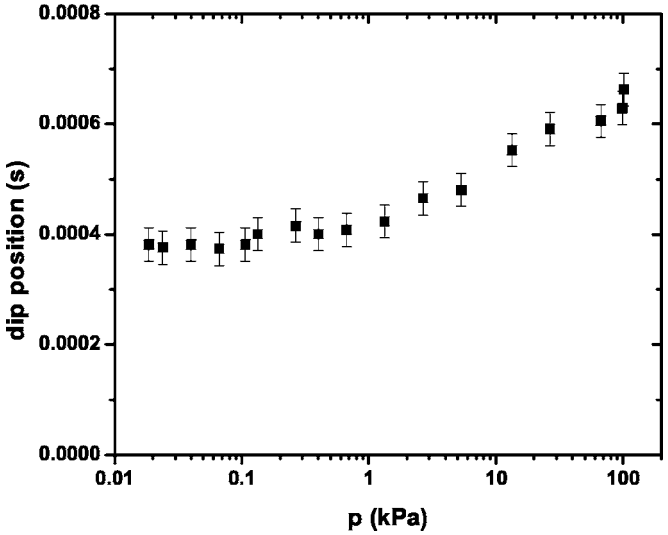

FIG. 9. Dip position as a function of pressure at $z=20$ cm.

In order to see how the cluster growth compares with pure gravitational stretching, the dip length is measured as a function of depth at four different pressures (Fig. 8). The dip positions have been converted into length scales by multiplying each of them with the local velocity that is obtained from Fig. 3. The gravitational stretch equation [Eq. (3)] is shown for each data set using the value for λ_0 found from the previous considerations, so there are no free fitting parameters. At $p=0.027$ kPa, the data is well fit by this equation. Unfortunately, the optical setup is not sensitive enough to pick up inhomogeneities above 10 cm depth. The fit for higher pressures agrees with the data until about $z=0.8$ m. At that point, the dip position grows larger than it would just with gravitational stretching.

Figure 9 shows the dip position in the autocorrelation as a function of pressure at constant depth $z=20$ cm below the nozzle. The dip position decreases with decreasing pressure until about $p\approx0.1$ kPa at which it stays constant down to the lowest available pressure 0.02 kPa. As we have seen before, the air has an appreciable effect on the cluster size. The dip changes by almost a factor of 2. Moreover, it shows that air has no effect below 0.1 kPa. Below that pressure the dip position remains constant over one order of magnitude in pressure.

V. DISCUSSION

Our data show that the clustering of a freely falling granular jet is influenced by the presence of air, but occurs even

at low pressures. At the lowest available pressure, $p=0.02$ kPa, the mean free path exceeds the particle size by a factor of 3, so air effects should be negligible. Moreover, at constant depth, the position of the first dip in the autocorrelation function, which is a measure of the typical size of the structure, stays constant below 0.1 kPa down to 0.02 kPa (Fig. 9). Therefore, air-grain interactions can be ruled out as the initial cause of the clustering.

It is worth noting that other granular phenomena that depend on the ambient pressure lose their pressure dependence below ≈ 0.1 kPa. Granular size separation in vibrated beds depends strongly on pressure when the grain size is small ($d \lesssim 500$ μm) [21,22]. It has been found that below 0.1 kPa air ceases to play a role. Another granular phenomenon that depends on air is heaping. The surface of a bed of small particles ($d \lesssim 600$ μm) starts to tilt when vertically vibrated [23]. It was found that heaping dramatically decreases below 1 kPa, since the mean free path of air becomes comparable to the grain size. This suggests that it is for this same reason that the dip position stops changing at low pressures in Fig. 9.

This experiment does not measure density, so cluster growth through agglomeration and the stretching of a cluster due to gravity cannot be distinguished. Nevertheless, the latter is always present, so it is sensible to compare the growth in cluster size with gravitational stretching.

The results indicate that the instability arises from fluctuations on the granular level at the nozzle. At the lowest available vacuum, where air effects are negligible, gravitation is the only external force acting on the particles. Indeed, the fit for gravitational stretching is good at these low pressures. Extrapolating the cluster growth back to the nozzle, the initial size is of the order of a grain diameter.

At higher pressures deviations from gravitational stretching are observed. The extrapolation yields an initial size that is almost a factor of 2 larger than at low pressures. Moreover, the jet starts to disintegrate into a cloud below some depth. This is presumably due to hydrodynamic interactions, since it is not observed at low pressures, at least in the observable range of depths.

Clustering is not observed for grain sizes larger than 200 μm. Visual inspection by strobing granular jets of larger particles did not reveal any inhomogeneities visible by eye. Smaller grains, on the other hand, give rise to strong clustering.

It is still unclear how these grain-sized fluctuations grow into clusters of several particles. After ruling out air-grain interactions, there are two possibilities left: Clustering is either induced by cohesive forces between particles or velocity correlations through inelastic collisions.

The cooling and eventual clustering of a granular gas of equal particles does not depend on the absolute size of the particles, but on the coefficient of restitution e. There are indications [24,25] that the coefficient of restitution may be size dependent. According to Ref. [25], $(1-e) \propto 1/d$, so smaller particles should cool down faster. It is unclear whether this size dependence could explain the absence of clustering in jets of large particles.

Another scenario is the clustering due to residual cohesive forces. Humidity and surface charges will always cause some residual attraction between particles. In this experiment cohesive forces are weak, though, as evidenced by the observed stretching of clusters during the fall. Particles that are in contact at the nozzle can come apart through collisions. Nevertheless, small attractive forces could play an important role near the nozzle where particles are still in contact. This scenario is also consistent with the trend that clustering disappears in granular jets of large and thus heavier glass particles.

Regardless of the clustering mechanism, an initial perturbation is required that acts as a seed for the cluster. Since gravity cannot initiate fluctuations and air-grain interactions have been ruled out, this perturbation is likely to come from the nozzle. One possibility might be that short-lived, transient arching events in the nozzle region provide tiny density variations that act as seeding events for later growth into clusters. This is consistent with the finding that the cluster size extrapolates to a few grain diameters at the nozzle.

VI. CONCLUSION

In contrast to ordinary fluids, granular flows lack surface tension and are discrete in nature. Despite these fundamental differences, a freely falling jet becomes unstable and forms drops in both cases. However, the physical origin of the instability in the granular case is quite different from its fluid counterpart.

The length scale, after tracing it back to the nozzle using the gravitational stretch equation, turns out to be of the order of a grain size at all pressures. This suggests that granular fluctuations at the nozzle set the cluster size. Moreover, it was shown that the surrounding liquid, in this case air, is not required for cluster formation. It does however, change the length scales by almost a factor of 2 and ultimately leads to the disintegration of the jet. The latter is not observed at low pressures.

These results might have implications on the clustering phenomenon found in suspensions [11,12]. Our experimental results show that fluctuations on the granular level can propagate downstream and thereby impose a length scale. This suggests that the granular nature of the sediment cannot be ignored and a continuous medium description may be inadequate.

This study also leaves some open questions: Clustering is not observed for glass spheres larger than 200 μm. This observation should give insight into the clustering mechanism which still remains unclear. How do fluctuations of single grains grow into clusters of many particles? Further studies are needed to answer this question.

The clustering of a freely falling granular jet is a granular instability that is initiated by fluctuations at the nozzle that are of the order of a grain diameter. These fluctuations grow into clusters downstream. The detailed structure of the clusters may reveal information about these fluctuations that are experimentally difficult to access otherwise.

ACKNOWLEDGMENTS

The author thanks H. Jaeger and S. Nagel for their support and guidance. I am grateful to X. Cheng, E. Corwin, M. Holum, J. Royer, and B. Chakraborty for useful discussions and suggestions. H. Krebs's expertise was invaluable to build the apparatus. This work is supported by MRSEC, No. DMR-0213745.

[1] J. Eggers, Rev. Mod. Phys. **69**, 865 (1997).
[2] G. W. Baxter, R. P. Behringer, T. Fagert, and G. A. Johnson, Phys. Rev. Lett. **62**, 2825 (1989).
[3] K. Schick and A. Verveen, Nature (London) **251**, 599 (1974).
[4] Y. Bertho *et al.*, J. Fluid Mech. **459**, 317 (2002).
[5] T. Raafat, J. P. Hulin, and H. J. Herrmann, Phys. Rev. E **53**, 4345 (1996).
[6] C. Veje and P. Dimon, Granular Matter **3**, 151 (2001).
[7] C. T. Veje and P. Dimon, Phys. Rev. E **56**, 4376 (1997).
[8] S. Thoroddsen and A. Shen, Phys. Fluids **13**, 4 (2001).
[9] D. Lohse, R. Bergmann, R. Mikkelsen, C. Zeilstra, D. van der Meer, M. Versluis, K. van der Weele, M. van der Hoef, and H. Kuipers, Phys. Rev. Lett. **93**, 198003 (2004).
[10] J. Royer *et al.*, Nat. Phys. **1**, 164 (2005).
[11] U. Schaflinger and G. Machu, Chem. Eng. Technol. **22**, 617 (1999).
[12] M. Nicolas, Phys. Fluids **14**, 3570 (2002).
[13] X-l. Wu, K. J. Måløy, A. Hansen, M. Ammi, and D. Bideau, Phys. Rev. Lett. **71**, 1363 (1993).
[14] R. Brown and J. Richards, Trans. Inst. Chem. Eng. **38**, 243 (1960).
[15] J. Duran, *Sands, Powders and Grains* (Springer, New York, 2000).
[16] S. McNamara and W. Young, Phys. Fluids A **5**, 34 (1993).
[17] I. Goldhirsch and G. Zanetti, Phys. Rev. Lett. **70**, 1619 (1993).
[18] N. V. Brilliantov and T. Pöschel, *Kinetic Theory of Granular Gases* (Oxford University Press, Oxford, 2004).
[19] *Handbook of Chemistry and Physics*, edited by D. R. Lide (CRC, Boca Raton, FL, 1997).
[20] P. Carman, *Flow of Gases Through Porous Media* (Butterworth Scientific, London, 1956).
[21] M. E. Möbius, X. Cheng, G. S. Karczmar, S. R. Nagel, and H. M. Jaeger, Phys. Rev. Lett. **93**, 198001 (2004).
[22] N. Burtally, P. J. King, and M. R. Swift, Science **295**, 1877 (2002).
[23] H. K. Pak, E. Van Doorn, and R. P. Behringer, Phys. Rev. Lett. **74**, 4643 (1995).
[24] L. Labous, A. D. Rosato, and R. N. Dave, Phys. Rev. E **56**, 5717 (1997).
[25] S. Luding, Ph.D. thesis, Universität Freiburg, 1994.